A Survey of Geomatics Solutions for the Rapid Mapping of Natural Hazards

I. Toschi, F. Remondino, T. Kellenberger, and A. Streilein

Abstract

Natural hazards demand a rapid assessment of the crisis situation and the use of Geomatics platforms, sensors and techniques can efficiently answer this need. Remotely sensed data can, in fact, provide a valuable source of broad scale information at each stage of the disaster management cycle, supporting scientists and authorities in the decision-making process. Geomatics-based procedures and techniques can be especially exploited in the emergency mapping domain for the extraction of reference (pre-event) and crisis (post-event) geographic data. The major challenges today concern the efficient selection (and integration) of the most fit-for-purpose mapping solution(s) and the development of automatic procedures to increase efficiency in data processing.

This survey article provides a review of the current optical remote sensing sensors (both satellite and airborne) for rapid mapping applications. Advantages and disadvantages are evaluated in order to support the selection process of the most appropriate means to gather the required information (i.e., significant and value-added data). Since valuable information should be delivered in a very short time, the management of time is defined as a priority and several solutions are discussed to pursue efficiency in both data acquisition and processing. With this in mind, the most significant issues affecting time in each step of the workflow and overall accuracy are analyzed and reported

Introduction

Emergency situations demand the development of an effective disaster management planning that can help to prevent exacerbation of hazardous situations. If the traditional approach was primarily focused on response to disasters as they occur, the emergency management is nowadays intended as an integrated cycle model (Figure 1). The "Disaster Management Cycle" consists of five main stages, described in Table 1 according to the definitions given in UN-SPIDER, UNEP (2012). Each of them may be supported through the use of Geomatics platforms, sensors and, techniques that provide valuable sources of information on a large scale (Joyce *et al.*, 2009a). Although data remotely sensed from satellite, aircraft and UAV (Unmanned Aerial Vehicle) cannot themselves result in reduced damage, they offer a privileged vantage point over the impacted area, thus facilitating the spatial understanding of the phenomenon and the gathering of objective and standardized information. Indeed, their use may facilitate better quality decisions and, in particular, support the activities of researchers, intervention teams and authorities actively involved in the immediate post-event phase, which is usually referred to as "Rapid Mapping" (Response or Early Impact, Table 1). In this regard, geomatics-based procedures are exploited for the "creation of maps, geo-information products and spatial analyses dedicated to providing situational awareness emergency management and immediate crisis information for response by means of extraction of reference (pre-event) and crisis (post-event) geographic information/data" (Emergency Mapping Guidelines, 2015). These geo-spatial products may feature different levels of resolution and accuracy that vary according to the final needs, especially in terms of delivery time.

In order to provide for a large resource of information and coordinate hazard response activities, several international initiatives have recently developed open-access platforms and information services based on Earth Observation (EO) systems. Among the others, the International Charter on Space and Major Disasters (The International Disaster Charter) is a collaboration between sixteen space agencies aimed at providing a unified system to access satellite imagery for disaster response. At the European level, the Copernicus Emergency Management Service (EMS) exploits Earth Observation (EO) satellite and *in-situ* data to deliver early warning information and risk assessments of floods (EFAS –European Flood Awareness System) and forest fire (EFFIS –European Forest Fire Information System). These services are expected to be soon extended at global scale, by means of the Global Flood

Table 1. The disaster management phases. Source: UN-SPIDER, UNEP 2012.

Disaster management	
Early warning	Prediction and timely recognition of imminent hazards, in order to alert people and allow them to get to safety.
*Early impact (Response – **Rapid mapping**)*	The provision of emergency services and public assistance during or immediately after a disaster in order to save lives, to reduce health impacts, to ensure public safety and to meet the basic subsistence needs of the people affected.
Recovery	The restoration, and improvement where appropriate, of facilities, livelihoods and living conditions of disaster-affected communities, including efforts to reduce disaster risk factors.
Mitigation	The lessening or limitation of the adverse impacts of hazards and related disasters.
Preparedness	The knowledge and capacities developed by governments, professional response and recovery organizations, communities and individuals to effectively anticipate, respond to, and recover from, the impacts of likely, imminent or current hazard events or conditions.

I. Toschi and F. Remondino are with the 3D Optical Metrology (3DOM) Unit, Bruno Kessler Foundation, Trento, Italy (remondino@fbk.eu).

T. Kellenberger and A. Streilein are with the Federal Office of Topography Swisstopo, Wabern, Switzerland.

Photogrammetric Engineering & Remote Sensing
Vol. 83, No. 12, December 2017, pp. 843–859.
0099-1112/17/843–859

doi: 10.14358/PERS.83.12.843

Awareness System (GloFAS) and the Global Wildfire Information System (GWIS). Furthermore, the EMS Mapping Service provides geospatial information based on satellite images, to assess the impact of worldwide natural and man-made disasters. A more general overview of the major Rapid Mapping services and recommendations for data types and techniques is given in the United Nations Platform for Space-Based Information Disaster Management and Emergency Response (UN-SPIDER). In addition to the main existing operating systems (*www.un-spider.org/space-application/emergency-mechanisms)*, the portal includes the "space application matrix" (*www.un-spider.org/space-application-matrix*), where the user can download relevant research papers according to the selected type of natural disaster and phase of the disaster management cycle.

All these initiatives demonstrate that geomatics-based techniques and products can be efficiently exploited to support crisis managers, civil protection and the other responders dealing with natural disasters and emergencies that require an immediate response. However, although there is a multiplicity of platforms and remote sensing sensors that could be used for data acquisition, the unpredictability and variety of hazards do not usually allow for a single all-encompassing solution to be adopted. Therefore, the choice of the sensor and the survey technique often remains the most critical decision.

Paper Objectives and Structure

This work reviews the major data acquisition solutions available in the market and explores their potentialities for rapid disaster assessment applications. The goal is to provide a useful survey to assist the decision-making and selection process when involved in hazard mapping and monitoring activities. Specifically, the identified hazards of interest include floods, mass movements (landslides, avalanches), earthquakes, fires, and storms.

Several review papers have been published in this field and their focus was mainly devoted to analyze the use of (a) volunteered geographic information, in the preparedness and mitigation phases (Klonner *et al.*, 2016); (b) geophysical techniques, in the risk assessment phase (Malehmir *et al.*, 2016); (c) satellite remote sensing sensors and data, in the mapping and monitoring phases (Voigt *et al.*, 2016; Joyce *et al.*, 2014; Joyce *et al.*, 2009b; Gillespie *et al.*, 2007; Tralli *et al.*, 2005); (d) UAV-based photogrammetry, in the risk monitoring and disaster management phases (Erdelj *et al.*, 2017; Petrides *et al.*, 2017; Gomez and Purdie, 2016); and remote sensing techniques for the management of specific disasters' types (Casagli *et al.*, 2017; Hoque *et al.*, 2017; Molinari *et al.*, 2017).

In this work the attention is primarily focused on both satellite and airborne optical imaging systems (platforms and sensors), since they offer significant advantages compared to ground-based survey. Indeed they offer a great ability to cover large areas within a short time and with limited site access constraints (e.g., debris blocking roads, roads washed out by storm surge, property and privacy considerations, security issues for a survey team.). Furthermore, since time management is paramount in rapid mapping situations, the most significant issues affecting the time in each step of the photogrammetric workflow are analyzed and possible methods to shorten it are proposed. Efficiency in both data acquisition and processing is discussed, with special regard to orthophoto production. Finally, a short review of relevant case studies is presented, with special focus on recent papers dealing with (a) application of satellite and airborne Geomatics solutions for the rapid mapping of natural hazards, and (b) time management in a typical airborne and UAV scenario.

Relevant Data and Requirements

When Geomatics is required to support the emergency management, the decision-making process should start from selecting the most relevant information (and derived value-added products) to be gathered. Within the rapid mapping domain, three types of assessment are mainly needed:

- situation assessment, to gather information on the magnitude of the disaster and the extent of its impact on the population, the infrastructures and the environment;
- needs assessment, to identify resources and services for immediate emergency measures;
- environmental impact assessment, to quantify environment damages and identify environmental issues to be considered while carrying out emergency operations.

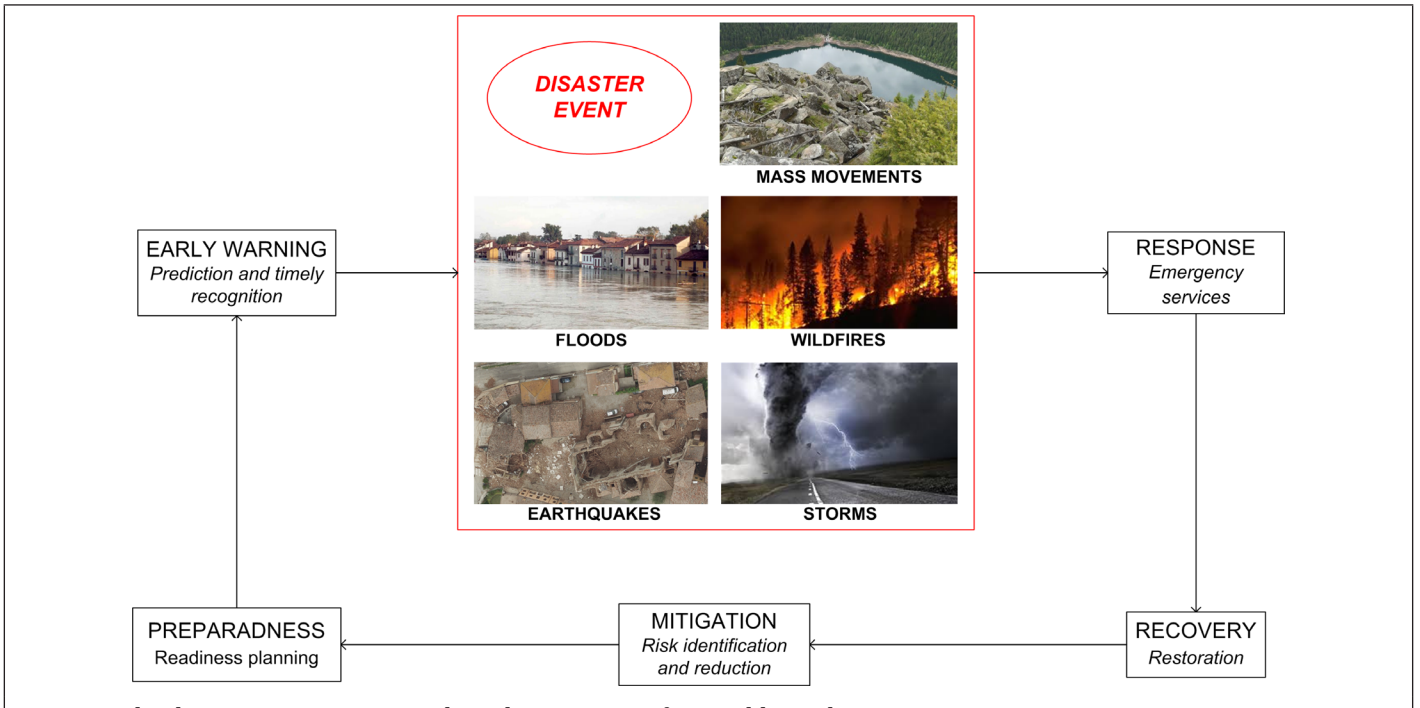

Figure 1. The disaster management cycle and main types of natural hazards.

Geomatics sensors and techniques can be efficiently adopted within both the situation and environmental impact assessments. In this regard, irrespective of the hazards type, particular attention should be paid to the collection of the most significant information or data, in accordance with standardization criteria and constraints (Boccardo, 2016). In particular, a consistent effort should be devoted to the processing phase in order to guarantee both the required quality (i.e., resolution and accuracy) and delivery time. Table 2 provides an overview that applies to all types of natural hazards.

Besides the most relevant data, further specific information should be collected according to the type of natural disaster. Table 3 offers a synthesis thereof, categorizing the required data as a function of the emergency type and acquisition time (i.e., prior to, during and immediately after the hazard event). In this regard, assessment activities should be tailored to (a) the pre-disaster phase (when disaster protection is possible), (b) the disaster phase (when possible), and (c) the post-disaster phase (Rapid Mapping).

Table 2. Relevant information to be collected and criteria/constraints to be fulfilled, irrespective of the hazards type.

Relevant information and data	Criteria and constraints
• size of the impacted area; • intensity of the damages; • zonation (i.e. different damage intensities within the impacted area); • location of victims.	• data should meet the required quality criteria (precision, accuracy and resolution) and clearly declare them; • presence of other areas potentially endangered. • value-added information should be extracted from the processed data, to support critical analyses and decision making; • data and value-added information should be delivered in a standard and documented format.

Table 3. Relevant information to be collected for each type of disaster pre(1)-, during(2) and post-event(3).

Type of disaster	Relevant information and data to be gathered
Earthquakes	(1) number of people to evacuate; (3) damage to infrastructures, especially critical transport infrastructures like roads, rails and airport; (3) damage to private and commercial buildings.
Mass movements (avalanches and landslides)	(1) presence of unstable snow layer, rocks, soil layer; (1) number of people to evacuate; (2) landslide extent; (2), (3) direction and speed of the movement; (3) information about the physical status and efficiency of critical infrastructures.
Floods	(1) number of people to evacuate; (2) flood extent; (2) volumetric data; (2) evolution of the event; (1), (2), (3) Digital Elevation Models (DEM) and Digital Terrain Model (DTM).
Storms	(1) number of people to evacuate; (3) information about the physical status and efficiency of critical infrastructures.
Wildfires	(1) number of people to evacuate; (1) potential fire ignitions; (2) fire extent and intensity; (2) hot spots detection. (2) direction of the fire and its evolution over time; (2), (3) observations of smoke conditions.

Geomatics Platforms and Sensors

Satellite Optical Solutions

Spaceborne remote sensing technology has been experiencing significant developments in recent decades. System parameters including spatial, spectral, and temporal resolution, have been improved, providing for an increasing availability of high-quality optical satellite images and, in some cases, a multiple daily coverage. These state-of-the art systems enable, in principle, the continuous monitoring of Earth's surface changes on all scales, from global, through national, to local levels. New multi-sensor solutions have been introduced that cover different parts of the electromagnetic spectrum and allow the acquisition of multiple data within a short time period. Much of these data are either freely available or provided at relatively low cost through international open-access infrastructures. This makes Earth Observation (EO) satellites a powerful means for supporting crisis mapping/damage assessment, including the rapid surveying of the location, scale and severity of the disaster impact (CEOS, 2015). In particular, the use of EO satellite data for rapid mapping applications provides several advantages, i.e., (a) accessibility to remote and hazardous areas without risk; (b) broad area coverage at low cost; (c) collection of consistent, standardized and comparable information on multiple scales. However, satellite images still suffer from a limited spatial resolution (usually, from 50 cm to few m), if compared to airborne solutions; furthermore, optical satellite data are weather dependent, with limited usability in case of significant cloudy coverage.

From a technological point of view, a spacecraft typically consists of two main components (Larson and Wertz, 1999), i.e. the bus and the payload. While the former functions as platform for the payload and controls the system parameters (i.e. attitude, electric power, temperature, communication and orbit), the payload is the sensor (or, group of sensors) that acquires the EO measurements. Focusing on satellite digital camera systems, the core sensing element still remains the linear CCD and, among the different imaging configurations, the most popular are pushbroom, whiskbroom and frame systems (Abdullah, 2013). Despite the rapid technological developments, the rather simple pushbroom sensor type is the most adopted camera concept for image formation, both in its basic form (i.e. a single chip of pixels that form the pushbroom framelet) and in its variations (i.e. more than one framelet in the focal plane or discontinuous flamelet). In terms of observation modes, state-of-the-art spacecraft can acquire images in various modalities (Figure 2): (a) spotlight mode (i.e. images for specific locations), (b) strip map mode (i.e. a continuous image acquisition applying a rotational attitude of the sensor), (c) wide range mode on the same location (i.e. a wide swath image captured using the forward, nadir and backward views), (d) 3D mode (i.e. stereo or triplet by forward, nadir, and backward views to obtain 3D information of the target area) and (e) skew mode (i.e. images acquired from a lateral direction and applying a rotational attitude to the sensor). By adopting these imaging configurations, both the observation of the most critical areas (hot spots) and the tracking of irregular coastlines and paths are made possible.

The most recent optical satellite solutions (missions and sensors) are reported in Table 4. Attention is focused on high and very high resolution sensors (Ground Sample Distance, GSD, below 10 m) launched over the past three years (2014 to 2017). A more comprehensive overview of EO satellites can be found by accessing the European Space Agency's satellite mission web portal (eoPortal) and the database provided by the Committee on Earth Observation Satellites (CEOS Database).

Airborne Optical Solutions

When high resolution imagery (from few centimetres to few millimetres), close range to target and high flexibility are needed, the use of airborne solutions can provide for a high

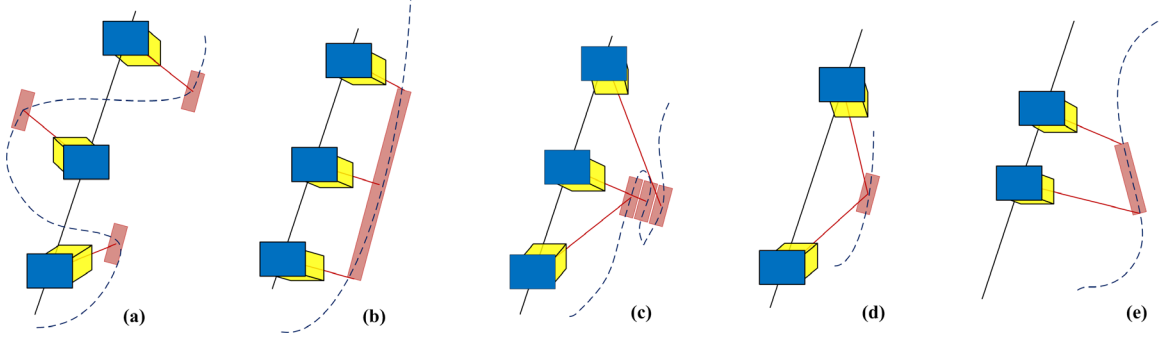

Figure 2. Layout of the different observation modes: (a) spotlight mode, (b) strip map mode, (c) wide range mode, (d) 3D mode and (e) skew mode.

Table 4. Satellite solutions: most recent optical satellite sensors with spatial resolution below 10 m. *Systems, specifically aimed at natural disasters' applications*, as identified in the ESA database (eoPortal available at https://directory.eoportal.org/web/eoportal/satellite-missions); (*) ground sample distance at nadir; (**) no stereo capability.

	Mission/ Sensor	Spectral bands	GSD(*) [m]	Swath width [km]	Revisit time	Inclination [°]	Altitude [km]
Launch year 2014	ASNARO/OPS	Panchromatic Multi spectral (6)	≤ 0.5 ≤ 2	10	-	97.4	504
	CBERS-3 & 4/PanMUX	Panchromatic Multi spectral (3)	5 10	60	3 days	98.5	778
	Deimos2/HiRAIS	Panchromatic Multi spectral (4)	0.75 4	12	4 day	98	630
	Gaofen-2/PMC-2(**)	Panchromatic Multi spectral (4)	0.8 3.2	23 (45 in combined configuration)	4-69 days (depending on the application)	97.9	631
	KazEOSat-1/NAOMI	Panchromatic Multi spectral (4)	1-2.5 4-10	From 10 km to 60 km at nadir depending on GSD and number of detectors	2 day	98.54	750
	KazEOSat-2/KEIS	RGB, Red edge, NIR	6.5	77	2 day	98	630
	WorldView-3/WV-3Imager	Panchromatic Multi spectral in VNIR (8) Multiband in SWIR (8)	0.31 1.24 3.70	13.1	1 m GSD: < 1.0 day 4.5 days at 20° off-nadir or less	98	617
Launch year 2015	*DMC-3/ SSTL-300 S1 Imager*	Panchromatic Multi spectral (4)	1 4	23	daily	97.8	651
	KOMPSAT-3/AEISS-A	Panchromatic Multi spectral (4) NIR	0.55 2.2 5.5	12	0.9 days (< 45° off-nadir) 2.7 days (< 20° off-nadir)	97.5	528
	LAPAN-A2/spaceCam c4000	RGB	5	3.5	-	8	650
	TeLEOS-1/TeLEOS-1 Imager	Panchromatic	1	12	12 to 16 hours	15	550
Launch year 2016	*ALOS-3* — *PRISM-2*	Panchromatic	0.8	50	-	97.9	618
	ALOS-3 — *HISUI*	Multi spectral (4) Hyper spectral	5 30	90 30			
	Diwata-1/HPT(**)	RGB, NIR	3	FOV of 1.9 km x 1.4 km	-	51.6	400
	FormoSat-5/RSI(**)	Panchromatic Multi spectral (4)	2 4	24	Every other day	98.28	720
	SuperView 1	Panchromatic Multi spectral (4)	0.5 2	12	4 days	98	530
	Göktürk-1/HiRI(**)	Panchromatic Multi spectral (4)	0.7 2.8	20	< 2 days	98.11	695
	WorldView-4/ SpaceViewTM110	Panchromatic Multi spectral (4)	0.31 1.24	13.1	≤ 3 days	98	617
Launch year 2017	*CartoSAT-2D* — *PAN*	Panchromatic	0.65	9.6	4 days	97.44	505
	CartoSAT-2D — *HRMX*	Multi spectral (4)	2	10			
	KhalifaSat/ KHCS	Panchromatic Multi spectral (4)	1 4	12	-	98.13	613

efficiency of data acquisition. The airborne remote sensing industry is experiencing an unprecedented diversity in the development of platforms and sensors. On one hand, light aircraft can now carry both frame and digital cameras, driven by the stresses placed by sensor manufacturers on aircraft's payload and power. On the other hand, many other types of platforms exist, that enable sensors to access remote and denied areas at operating altitudes. Indeed, rapid mapping interventions after disaster events can now be performed using data acquired by a number of different airborne geomatics solutions.

Within the aircraft industry for mapping purposes, twin-engine platforms still represent the most adopted solution for data collection. Performance gains in airspeed and power allow for increased operating altitudes to be reached and maintained, thus ensuring broad area coverage capabilities and higher efficiency. A fully digital system including one or, usually, more sensors (e.g. cameras, lidar, navigation and positioning systems, data storage, and management units) can be supported by modern aircraft, thanks to their higher weight and power limits. At the same time, the advent of high-quality small-format digital cameras is now pushing the use of lighter and less expensive single-engine aircraft. These platforms enable slow, low-altitude and single-person operations with modest payloads, providing for a good compromise between a limited initial investment cost and the collection of high quality products. As rapid mapping platforms, aircraft can provide for high spatial resolution imagery (up to few cm) and high efficiency of data acquisition (i.e., larger area coverage per unit of time). On the other hand, manned aircraft are limited by several constraints in the flight management (minimal flight speed and altitude, no curves and corridors) and require rigorous flight planning. Finally, crew duties limit their mission to 4 to10 hours, and they are hardly operative during hazardous weather conditions.

When a close-range to target scenes is needed, helicopter platforms are generally preferred. They can feature both internally- and externally-mounted sensors' configurations and, in the former case, they enable a good temperature and environmental control. Potentially, they also allow the adoption of hand-held acquisition systems, as demonstrated in (Skaloud *et al.*, 2006; Calvari *et al.*, 2004; Vallet and Skaloud, 2004). Their good maneuverability (even in case of bad weather conditions), freedom to operate, and easy access in congested airspace make them an efficient mapping means for quick response applications. In particular, helicopters are usually preferred when flight characteristics require low altitude, low speed, or following curves/corridor trajectories; therefore, they are ideal for the detailed evaluation of hot spots or corridor scenarios that are difficult to access with fixed-wing aircraft. However, if compared to aircraft, they can provide for a lower coverage capacity per unit of time. Finally, helicopters could be a costly solution.

A lower-cost solution is represented by Unmanned Aircraft Systems or Vehicles (UAS or UAV), that come nowadays in many different forms and with a variety of mapping capabilities. They are usually categorized by size, weight, flying altitude, payload, and endurance, and their increasing use for remote sensing applications is proved by an extensive body of literature (Nedjati *et al.*, 2016; GIM-International UAS edition, 2016; Gomez and Purdie, 2016; Colomina and Molina, 2014; Nex and Remondino, 2014). The rapid development of UAV technologies and the miniaturization of on-board equipment provide the users with several solutions: among those, the most common platforms adopted in photogrammetry and remote sensing applications are listed in Table 5. Their use for the rapid provision of useful information in support of disasters is driven by their high flexibility and maneuverability, capability of very high image resolution (up to few mm), adaptability to fly at different altitudes and ability to access remote and dangerous environments without any risk for the pilot/operator. Both vertical and oblique imaging is allowed, particular with multi-rotor platforms. Major disadvantages concern endurance, payload, and area coverage limitations.

With regards to the payload component, the evolution in digital technology has provided for a suite of remote sensing sensors that can be efficiently used for rapid mapping applications.

Focusing on airborne digital camera systems, a great variety of solutions are available on the market. Table 6 lists the most common systems, classified as small, medium, and large format digital cameras. Among them, medium format digital cameras nowadays offer the best flexibility in terms of imagery acquisition for rapid response. This category is generally defined as single sensor-based camera system with an image resolution ranging from 30 MPX to about 100 MPX, and it currently represents the fastest growing segment of the airborne mapping market. Practically all of the vendors offer products in this category, whose performance almost matches that of the first-generation large format camera systems. Medium-format cameras are usually oriented to support applications where moderate to high resolution is required and/or to integrate multi-sensors airborne platforms as companion sensors for lidar systems. A good review of early and most recent systems can be found in (Edwards *et al.*, 2013; Remondino, 2011; Petrie, 2010; Grenzdörffer, 2008).

A new technology which is rapidly maturing and entering the market of airborne mapping sensors is constituted by airborne digital multi-camera systems. With respect to the design, more recent systems are a combination of two cameras (fan configuration) or four cameras (Maltese-cross architecture), i.e., one photogrammetric nadir viewing camera combined with four tilted cameras with forward-, backward-, left- and right-viewing directions. The latest solutions integrate an increasing number of cameras, such as the MIDAS Octoblique that adopts one vertical and eight oblique cameras spaced at 45° around a complete 360° view. With respect to their spectral characteristics, oblique sensor heads usually acquire the visible (RGB) bands, although some recent models also include the NIR (Near Infrared) channel for the nadir-looking sensor head. The advantages of oblique imagery lie in its simplicity of interpretation and in its inherent capacity to reveal building façades and footprints. Consequently, this encourages the use of oblique images in rapid mapping applications, although multi-camera systems still represent bulky, heavy, and costly solutions and require a proper flight plan to be carried out in order to cope with efficiency issues during the pre-processing phase. Table 7 lists the most recent multi-camera systems and their characteristics; literature review and best practices for mapping applications can be found in (Remondino *et al.*, 2016; Remondino and Gerke, 2015).

Specifically for UAV, several small and medium format digital camera solutions have been recently developed, ranging from the visible band, to the NIR, up to the Thermal Infrared (TIR) and microwave systems. The maturation of visible-spectrum cameras allowed high-quality, high-resolution and low-cost solutions to become suitable for micro, mini and tactical UAV payloads. Besides RGB cameras, several small, commercial multi-spectral sensors exist, along with hyperspectral cameras dealing with imaging narrow spectral bands over a continuous spectral range. In this regard, the huge amount of information that can be extracted from the spectral data about objects on the ground allows image classification to be performed with higher accuracy. Finally, there has been noticeable progress in thermal imaging miniaturization in recent years, providing for low-weight and small-size sensor solutions that can be efficiently used for remote reconnaissance and hazard mapping (e.g., fire monitoring). The most common small and medium format digital cameras for UAVs are summarized in Table 8, particularly distinguishing between visible-band, near-infrared, multispectral, hyperspectral, and thermal optical sensors.

Recent years have also seen the increasing use of active 3D imaging systems (such as lidar - Light Detection and Ranging) both in the commercial sector and by research groups. Focusing on airborne sensor solutions, airborne laser scanner (ALS) represents an extremely powerful technique to acquire direct range measurement of terrain (Flood, 2001). Lidar is now widely used to generate high-quality, very high resolution DEMs (Digital Elevation Models) for terrain analysis, to map landslides and debris-flows, to monitor mass movements, and to refine surface flow models. However, despite the general availability of intensity information, lidar lacks the visual interpretation of data (only geometry is recorded, no RGB), which is useful for both manual and automated processing. Therefore, the use of airborne laser scanners is usually combined with that of medium-format digital cameras, offering several advantages compared to classical airborne techniques: vegetation penetration, direct digital terrain/surface model (DTM/DSM) generation, DTM/DSM integration with RGB information and orthophoto generation.

Table 5. UAV solutions: most common UAV platforms adopted in photogrammetry and remote sensing applications (*) Dimensions given as wingspan, l × h and diameter for fixed-wing, rotary-wing and multi-rotor uav's, respectively

	Model	Manufacturer	Dimensions(*) [m]	Max. payload [kg]	Endurance [minutes]	Max. speed [km/h]
Fixed-wing unmanned aircraft	swinglet CAM	SenseFly	0.80	0.5 (weight incl. supplied 18.2 Mpx camera)	30	36
	GEOSCAN 101	Geoscan	1.30	0.5	60	60
	UX5	Trimble	1	2.5 (weight incl. supplied 24 Mpx mirrorless APSC)	50	80
	Pteryx Pro	Trigger Composites	2.4	1	120	45-55
	SIRIUS	MAVinci	1.63	Different options and add-ons are available	50	65
	Kahu	Skycam	2.2	3.9 (total weight, optical and IR cameras available)	120	100
	Bramor rTK	C-Astral	2.3	1	150	83
	EasyMap	Trigger Composites	0.90	0.35	45	90
	BIRDIE	FlyTech UAV	0.98	0.5	30	20
	Freya	SmartPlanes	1.20	0.6	60	70
	Ikhana	NASA	20	950	30	-
	Bat-3	MLB	1.8	2.27	360	104.6
	ScanEagle	Boeing Insitu	3.1	3.11	over 1200 (20 hrs)	150
	Heron	Israel Aerospace Industries	16.6	250	3120 (52 hrs)	207
	RQ-4 Global Hawk	Northrop Grumman	39.9	540	over 1920 (32 hrs)	629
Rotary-wing unmanned aircraft	Unmanned K-MAX®	KAMAN Aerosystems	16 x 15.8	2722	180	148
	RMAX	Yamaha	2.75 x 1.8	28	45-60	40
	Scout B1-100	Aeroscout GmbH	3.3 x 1.3	18	90	80
	BICOPT CH	weControl	1.95 x 0.90	10	90	50
	SR200 SR100 SR30	Rotomotion	2.79 x 0.86 1.470 x 0.685 1.638 x 0.622	22.7 8 8.5	300 20 90	80 79 40
	AF25B	CopterWorks	1.778 x 0.711	11.3	50-55	96.6
	UVH-29E	SURVEYOR-H	1.6 x 0.55	0.7 (with full fuel tank)	180	120
	Avenger-E Avenger-G	Homeland Surveillance & Electronics LLC	1.47 x 0.51 1.47 x 0.51	4.5 4.5	25-45 60-120	- -
Multi-rotor unmanned aircraft	MULTIROTOR G4 Recon One	MULTIROTOR	1.18	5-5.3 (incl. camera suspension and flight battery)	50-70	30-40
	Zero 1600 Hexacopter	Zero Tech	1.6	6	60	28.8
	MD4-1000	Microdrones	1.03	1.2	87.6	43.2
	HT-8 (Octocopter)	HEIGHT TECH	0.90	2.65 (incl. camera, mounting and battery)	20	70
	Aibot X6	Aibotix	1.05	2	20	50
	AscTec Falcon 8	Ascending technologies	0.77	0.8	12-22	57.6
	HexaKopter	MicroKopter	-	0.8-1	36	36
	RiCOPTER	RIEGL	1.92	16	30	60
	albris (eXom)	senseFly	0.80	1.8 (incl. battery, TripleView head payload & shrouding)	22	43
	Aeryon SkyRanger	Aeryon	1.02	1	50	65

While the use of lidar technology together with medium-large format cameras, also in multi-camera configurations (see Leica CityMapper in Table 7), is now common in airborne photogrammetry applications, their transfer to UAV for remote sensing and mapping purposes is still challenging, either due to the difficult trade-offs between performance and size or cost of lidar, or due to the effect of flight dynamics on the measurement process. However, future electronics innovations are expected to reduce the cost, size, and weight of these payloads, while increasing their performance and, as a consequence, their use on UAV platforms.

Finally, several commercial multi-sensor solutions have been recently developed, in order to provide the user with all-in-one systems (including usually both hardware and software) for rapid mapping tasks. They commonly comprise mapping sensors (active and/or passive 3D imaging systems), navigation/positioning sensors (IMU/GNSS) and a control unit that synchronizes and integrates the acquisition of geometric/positioning information. All sensors are integrated on a moving platform, such as aircrafts, helicopters, or UAVs. The system is often complemented with a software solution that processes the raw data into value-added products (e.g., georeferenced orthophoto). The most recent commercial solutions include (Figure 3): Trimble/Applanix DSS 500, Helimap System®, Siteco Sky-Scanner, TopoDrone 4Scight, and senseFly eBee RTK.

Table 6. Airborne solutions: most common airborne digital cameras and systems, with special focus on medium-format (MF) solutions. (*) If the system includes more than one frame.

	Model	Manufacturer	Image resolution [MPx]	Pixel size [µm]	Sensor type and no. of frames(*)/ lines	Spectral bands
Small format	EnsoMosaic system: • Canon EOS 6D • Canon EOS 5Ds R • Hasselblad H4D-60 • Rikola Hyperspectral	MosaicMill	 20 51(MF) 60 (MF) 1010×1010 px	 6.5 4.1 4.4 5.5	 Frame Frame Frame Frame	RGB RGB RGB default spectral range 500 – 900 nm
	Geoniss system: • Nikon D3X • Hasselblad H3D	Geoniss	 24 22, 39(MF)	 6 9, 6.8	 Frame Frame	RGB RGB
	VisionMap systems: • MIST-U • MIST-IR • MIST-G	VisionMap	 12.6 1.3 1.3 (IR) – 8.1 (RGB)	 7.4 15 15 (IR) -5.5 (RGB)	 Frame Frame Frame	RGB IR RGB and IR
	CS-6500	Optech	29	5.5	Interline Transfer	RGB-panchromatic
	Trible Aerial Cameras P25	Trimble	22	9	Frame	RGB
Medium format	Wehrli/Geosystem pushbroom systems: • 3-DAS-1 • 4-DAS-1	Wehrli/ Geosystem	8002 px per line	9	 Linear (3) Linear (4)	RGB RGB and NIR
	Trimble Aerial Cameras: • P45+ • P65+ • IQ180	Trimble	 39 60 80	 6.8 6 5.2	 Frame Frame Frame	 RGB RGB RGB
	CS-10000	Optech	80	5.2	Frame	RGB
	DigiCAM: • DigiCAM • Dual DigiCAM	IGI	 40, 50, 60, 80 76, 98, 118	 6, 6, 6, 5.2 6.8, 6, 6	 Frame Frame	 RGB or CIR RGB or CIR
	Leica-RCD100	Leica Geosystems	39	6.8	Frame (1 or 2 CH39 camera heads)	RGB or CIR
	RMK D Camera System	Intergraph	37	7.2	Frame (4 camera heads)	RGB,NIR
	UltraCam-Lp system	Vexcel Imaging	92 (48x2,PAN), 24 (MS)	6	Frame (4)	PAN, RGB,NIR
Large format	DMC II 250	Z/I Imaging	250 (PAN), 4x42 (MS)	5.6 (PAN), 7.2 (MS)	Frame (4 PAN, 4 MS)	PAN, RGB, NIR
	UltraCam-Xp system	Vexcel Imaging	196 (PAN), 22 (MS)	6	Frame (9 PAN, 4 MS)	PAN, RGB, NIR
	UltraCamEagle system	Vexcel Imaging	262 (PAN), 29 (MS)	5.2	Frame (9 PAN, 4 MS)	PAN, RGB, NIR
	UltraCam Condor	Vexcel Imaging	196 (RGB), Lower resolution PAN	-	Frame	PAN, RGB, NIR
	Leica ADS80	Leica Geosystems	12000 px per line	6.5	Linear (4 PAN, 8 MS)	PAN, RGB, NIR
	Triple DigiCAM	IGI	175 or 145 or 112	6	Frame	RGB or CIR
	Trimble Aerial Camera x4	Trimble	135 or 210	-	Frame (4 camera heads)	RGB

Table 7. Airborne solutions: most common airborne oblique multi-camera systems. (*) N: Nadir; O: Oblique; (**) Leica Hyperion Lidar Unit

	Model	Manufacturer	No. of sensors(*)	Image resolution [px]	Pixel size [µm]	Spectral bands	Focal length(*) [mm]
Maltese-cross configuration	Leica RCD30 Oblique	Leica Geosystems	1 (N) + 4 (O)	(5x) 10320×7752	5.2	RGB, NIR	50 (N), 80 (O)
	Leica CityMapper	Leica Geosystems	1 (N) + 4 (O) + LiDAR unit (**)	(5x) 10320×7752	5.2	RGB, NIR	80 (N), 150 (O)
	UltraCamOsprey I	Vexcel Imaging	1 (N) + 6 (O)	11674×7514 (N) 6870×4520 (O)	6 (N) 5.2 (O)	RGB, PAN,NIR	51 (N), 80 (O)
	UltraCam Osprey Prime	Vexcel Imaging	1 (N) + 4 (O)	11674×7514 (N) 8900×6650 (O)	6	RGB, PAN,NIR	80 (N), 120 (O)
	UltraCam Osprey Prime II	Vexcel Imaging	1 (N) + 4 (O)	13470×8670 (PAN-N) 6735×4335 (RGB-N) 10300×7700 (RGB-O)	5.2	RGB, PAN,NIR	80 (N), 120 (O)
	Pictometry	Pictometry	1 (N) + 4 (O)	(5x) 2672 x 4008	9	RGB	65 (N), 80 (O)
	Midas 5	Track'Air/MIDAS	1 (N) + 4 (O)	(5x) 5616 x 3744	6.4	RGB	80 (N), 120 (O)
	Penta DigiCAM	IGI	1 (N) + 4 (O)	2 options (5x): 10328×7760 11608×8708	5.2 4.6	RGB RGBI, RGB, CIR, NIR	90
Block configuration	Quattro DigiCAM	IGI	4	2 options (4x): 20550×14700 23350×16400	5.2 4.7	RGBI, RGB, CIR, NIR	90
	AIC	Optron/Trimble	4	(4x) 7228×5428	6.8	RGB, CIR	60 and 100
	Octoblique Midas	Track'Air/MIDAS	9	(9x) 8688×5792	4.1	RGB	-
Fan configuration	A3 Edge	VisionMap	2	(2x) 4864×3232	7.4	RGB, RGB+NIR	300

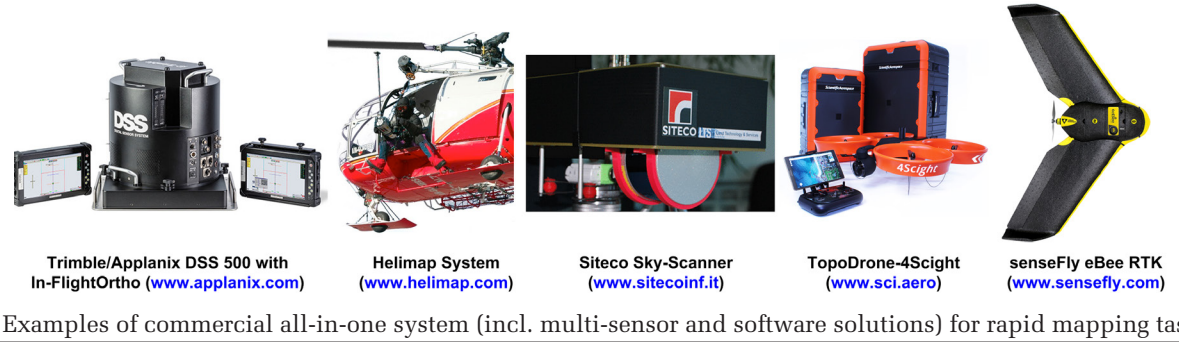

Trimble/Applanix DSS 500 with In-FlightOrtho (www.applanix.com) | Helimap System (www.helimap.com) | Siteco Sky-Scanner (www.sitecoinf.it) | TopoDrone-4Scight (www.sci.aero) | senseFly eBee RTK (www.sensefly.com)

Figure 3. Examples of commercial all-in-one system (incl. multi-sensor and software solutions) for rapid mapping tasks.

Summary

The main advantages and disadvantages associated with each data acquisition technology are summarized in Table 9. A complementary data source to EO satellites and airborne data can be represented by land-based systems, e.g., back-pack solutions, van-based mobile mapping systems, and handheld digital cameras. For instance, ground-based solutions have been adopted, either alone or coupled with airborne techniques, for the rapid mapping of earthquakes (Chiabrando *et al.*, 2017), lava flows (Coltelli *et al.*, 2017), wildfires (Perez-Mato *et al.*, 2016) and flash floodS (Smith *et al.*, 2014). Generally, they are useful for mapping applications at individual building and neighborhood levels and often represent the best solution for collecting images of the street facing side(s) of the buildings. However, ground-based imagery acquisition can be hindered by site access limitations (e.g., downed trees, power lines, and other debris blocking the roads), private property and privacy considerations, as well as security issues for the in-situ damage survey team. Therefore, in case of large natural hazards and disasters, they are not normally employed, particularly in the first hours after the event.

Finally, Table 10 provides a summary that links the different hazards' types with the relevant information needed for disaster mapping and the technologies or products that can be adopted to efficiently deliver those data to the end-users (e.g., disaster organizations and rescue groups).

Efficiency

When it comes to the rapid mapping of natural hazards, the choice of the most appropriate means (i.e., platform and sensor) to gather the required information (i.e., significant and value-added data) is not enough. Valuable information should be delivered in a very short time span, usually in the first hours after the event. Thus, time management is a paramount issue in the whole workflow leading to the delivery of the final product, from raw data acquisition and processing, to result dissemination. Depending on the selected remote sensing technique, the most significant issues affecting time in

Table 8. Airborne solutions: most common small and medium format digital cameras for UAVs. (*) MF/SF: medium/small format; FP: focal plane shutter; LS: leaf shutter.

	Model	Manufacturer	Image resolution [MPx]	Pixel size [µm]	Weight [kg]	Notes(*)
RGB cameras	iXA 160 iXA 180	Phase One	60.5 80	6 5.2	1.75	MF CCD sensor, speed 4000 s-1 (fp)
	P65+ IQ180	Trimble	60 80	6 5.2	1.50	MF CCD sensor, speed 1000 s-1 (ls)
	H5D-60	Hasselblad	60	6	2.29 (incl. 80mm lens)	MF CCD sensor, speed 800 s-1 (ls)
	Sony Alpha NEX-7	Sony	24.3	3.9	0.4	SF CMOS sensor, speed 4000 s-1 (fp)
	Sony Alpha NEX-5N	Sony	16	4.7	0.27	SF CMOS sensor, speed 4000 s-1 (fp)
	Sony Alpha a6000	Sony	24	3.9	0.34	SF CMOS sensor, speed 4000 s-1 (fp)
	GXR A16	RICOH	16.2	4.8	0.35	SF CMOS sensor, speed 3200 s-1 (fp)
Multispectral cameras	Micro-MCA6	Tetracam	1.3	5.2	0.53	CMOS sensor, spectral range 450 – 1000 nm (4-6-12 bands)
	Macaw	Tetracam	1.3	4.8	0.55	CMOS sensor, spectral range 450 – 1000 nm (6 bands)
	Condor3-UAV Condor5-UAV	Quest innovations	2.8 7	4.06 6.45	0.35 (incl. 12.8mm lens) 1.45/1.95 (incl. 50/15mm lens)	CCD sensor, spectral range 400 – 1000 nm (3-5 bands)
	MAIA	SAL Engineering srl/EOPTIS srl	(9x) 1.2	3.75	0.42	Global shutter, CMOS sensor, spectral range 390 – 950 nm (9 bands)
	RedEdge	MicaSense	(5X) 3.6	-	0.18	Global shutter, 5 spectral bands: blue, green, red, red edge, near IR (narrowband)
	Parrot Sequoia	MicaSense	(4x) 1.2 - spectral camera 16 – RGB camera	3.75	0.14	Global shutter, spectral range green, red, red edge, near IR (narrowband)
Hyperspectral cameras	Hyperspectral Camera	Rikola Ltd.	1010×1010 px (max spectral image dim.)	5.5	0.72	CMOS sensor, spectral range 500 – 900 nm (other options available) spectral bands 380 (max), spectral resolution 10 nm
	Micro-Hyperspec X-series NIR	Headwall Photonics	-	30	1.03	InGaAs linear sensor, spectral range 900 – 1700 nm spectral bands 62, spectral resolution 12.9 nm
Thermal cameras	Tau 2 640	FLIR	640x512 px	17	0.07	Uncooled VOx, spectral range 7.5 – 13.5 µm thermal sensitivity ≤50 mK
	Miricle 307K-25	Thermoteknix Systems Ltd.	640x480 px	25	0.11	Amorphous Silicon, spectral range 8 – 12 µm thermal sensitivity ≤50 mK

each step of this workflow and possible methods to shorten it should be considered. A successful project plan, indeed, must meet the project objectives at minimal cost, namely in terms of timing.

This concept, if applied to a photogrammetric project, would generally translate to the formulation of the acquisition efficiency as the average area surveyed per unit of time, for a given GSD. In particular, focusing on a typical airborne scenario, the following main project parameters should be carefully defined:

- Geographical limits and shape of the area of interest (AOI): its geometry has a significant impact on the acquisition efficiency, since a rectangular AOI requires a lower number of flight turns, if compared to an irregular AOI.
- Spatial accuracy (and scale) of the final map: the accuracy specification, both horizontal and vertical, plays an essential role in determining the cost of a photogrammetric project. In particular, it requires balancing several considerations in the selection of the aerial camera, the flight height above the ground (H) and the average image scale (1/S). These factors are, as known, related by the following formula:

$$\frac{1}{S} = \frac{\text{pixel size}}{\text{GSD}} = \frac{\text{focal lenght}}{H} \quad (1)$$

Obviously, the smaller the image scale, the fewer images will be needed to cover the mapping area, with a resulting time reduction. Thus, the objective in the planning should be to determine the smallest image scale that will meet the accuracy requirements of the photogrammetric project. Since the equipment availability is usually limited or constrained, the choice of the flying height becomes the most significant design parameter and should be defined by balancing both accuracy requirements and practical restrictions.

- Design of the flight plan: The photogrammetric mapping requires that a stereoscopic coverage is provided for the entire AOI through the definition of the optimal overlap between successive exposures in the forward direction (usually called endlap or along-track overlap) and between adjacent flight lines (usually called sidelap or across-track overlap). Most specifications for aerial photogrammetry require that the endlap be in the range 57-65 percent and the sidelap exceed the minimum value of 30 percent. This scenario mainly depends on the terrain relief (that causes displacements in the images) and on the

Table 9. Advantages and disadvantages of different types of data acquisition platforms.

Platform	Advantages	Disadvantages
Satellite	• accessibility to remote and hazardous areas without risk; • broad area coverage; • collection of consistent, standardized and comparable information on multiple scales (from local to global); • low cost.	• limited spatial resolution (from 50 cm to few m); • limited temporal resolution (data availability dependent on revisit time); • weather dependent (limited usability in case of significant cloudy coverage).
Aircraft	• high spatial resolution (up to few cm); • high efficiency of data acquisition (faster flight speed and higher altitude allow larger area coverage per unit of time); • both vertical and oblique perspectives.	• flight planning is required; • minimal flight speed and altitude are required; • no curves and corridors (possible flying problems in difficult scenarios, e.g. small valleys); • high cost; • limited flight duration due to crew duties; • no flight in dangerous weather conditions.
Helicopter	• close range to target (hot spots assessment); • low altitude, low speed allowed; • possibility to fly curves and corridors; • good maneuverability; • freedom to operate; • easily access in congested airspace.	• lower coverage capacity per unit of time; • high cost; • limited flight duration due to crew duties; • no flight in dangerous weather conditions.
UAV	• high flexibility and maneuverability; • very high image resolution (up to few mm); • adaptability to fly at different altitudes (e.g. low flight under cloud); • ability to access remote and dangerous • environments without risk; • both vertical and oblique perspectives; • low cost.	• limited payload; • limited endurance; • restricted area coverage.
Land-based	• high details at single building level and on building's facades; • flexibility; • low cost.	• limited field of view and area coverage; • site access limitations; • prone to damage and failure; • security issues for the damage survey team.

Table 10. Summary of the different hazards types, the relevant information needed for disaster mapping and the technologies (and derived products) that can be adopted to provide for such data.

Type of disaster	Information	Technology (and product)	Remarks
Earthquakes	• building conditions (intact, partially damaged, collapsed, etc.); • road network conditions; • research of survivors.	• oblique imagery; • classical nadir imagery; • thermal imaging.	• in case of dense vegetation canopies, lidar is able to penetrate the vegetation and provide a view of the bare terrain (useful for mapping the fault line traces). • oblique imagery is useful to reveal damages on building façades and footprints.
Mass movements (avalanches and landslides)	• locations of buried people; • zonation of impacted area and infrastructures; • existence of unstable snow layer.	• thermal imaging (if victims are close to surface); • nadir and oblique imagery; • lidar.	• photogrammetric and lidar data are also used to provide high-quality slope parameter data and volume of material moved (by DEM differentiating).
Floods	• impacted area; • elevation, surface and volumetric data.	• nadir imagery (orthophoto); • lidar (DEM, DTM and DSM).	• lidar data are also used to derive surface roughness layers to incorporate into hazard models.
Storms	• building conditions (intact, partially damaged, collapsed, etc.); • road network conditions; • research of survivors.	• oblique imagery • classical nadir imagery • thermal imaging.	• lidar data can be used to derive high spatial resolution DEM/DTM for defining geomorphological features and for modelling the flow of water.
Wildfires	• hot spots localization; • direction of the fire and its evolution over time • firefight efficiency assessment	• RGB and thermal imaging.	• IR is the most useful wavelength for day and night wildfire assessment: • mid-IR detects strong radiation emissions; • far-IR detects the naturally emitted radiation; • NIR can be used to provide more accurate data by eliminating false-positive (bright objects detected during the day).

strategy selected for the subsequent aerial triangulation (AT). Obviously, the acquisition time decreases in parallel with the sidelap, since the smaller it is, the fewer flight lines are needed to cover the mapping area. On the other hand, the endlap has no direct impact on the time for data acquisition, being the flying speed almost constant; however, a lower endlap will reduce the number of exposures, i.e., the number of images that should be processed.

- Operational flight parameters, such as the flight speed, the turn pattern and the time set for the initialization point (IP): while the former depends on many factors, e.g., platform performances, forward motion compensation limits, standard speed according to economic and environmental issues, exposure time, image storage time, etc., the latter are mainly influenced by the aircraft characteristics and the pilots capacity.
- Design of the ground control, i.e., the number and spatial configuration of horizontal and/or vertical control points required for scaling and leveling the model: additional ground control is usually required in forms of

checkpoints to evaluate the accuracy of the aerial triangulation. This planning is mainly influenced by the strategy selected for processing the aerial block and would benefit (in terms of cost and time reduction) from the adoption of a GPS-supported or a direct georeferencing approach.

Based on these remarks, Table 11 lists the main issues affecting time management in the image acquisition step and proposes possible approaches to increase efficiency.

Besides acquisition efficiency, the photogrammetric project should be planned in order to provide for the highest post-processing efficiency, that is usually defined as as the time required to process a given number of images (computed as sum of single time values associated to the processing steps). Obviously, the post-processing time first depends on the available computing capacities (i.e. hardware and software). Second, the number of images and their size (expressed in terms of geometric and radiometric resolution) represent key-factors to define the dimension of a photogrammetric project. However, the most important factor affecting the post-processing time still remains the strategy adopted to retrieve the camera exterior orientation parameters. Advancements in Global Positioning System (GPS) hardware and software has led to the developments of alternative methods to the conventional aerial triangulation, that was originally dependent on a sufficient number of 2D/3D control points well distributed over the entire AOI. If the incorporation of GPS-derived camera position data in the bundle block adjustment (i.e., GPS-supported aerial triangulation) allows for saving time and cost by reducing the need for ground control; the highest gain is achieved by skipping the triangulation on the block of images through direct georeferencing (DG). In this case, in fact, exterior orientation parameters are directly derived from GPS/IMU data, after computing and applying the boresight and offset correction to the attitude and position data. Obviously, the applicability of this approach depends on the accuracy of the available GPS/IMU data and on the quality requirements that the final product should meet. In this regard, many tests have been performed to assess the accuracy and reliability of Direct Georeferencing (DG) for rapid mapping purposes, and two relevant case studies will be reviewed in a following Section.

Based on these remarks, Table 12 lists the main issues affecting time management in the postprocessing steps and proposes possible approaches to increase efficiency. Here, attention is mainly focused on airborne digital orthophoto production, since it is normally the most common and versatile mapping product.

Clearly, one should consider that faster and/or simplified processes (or eventually the skipping of processes) usually affect the final orthophoto quality (in terms of radiometry, seamlines, and accuracy). Therefore, a decent balance should be found between time shortening and meeting the required technical specifications. When dealing with orthophoto production, the latter are usually expressed in the form of radiometric and spatial (or positional) quality. In particular, radiometric requirements may be critical if the image product is used for gathering specific attribute information out of the scene content. Indeed, features extraction requires a good radiometric quality that is quantitatively measured by aspects such as the dynamic range, the amount of noise, and the "sharpness" of the imagery. At the same time, when measurements are to be taken on the generated ortho-rectified products, spatial requirements should be also considered. In this regard, the accuracy is normally stated in the horizontal plane and evaluated by comparing the image-derived 2D coordinates of well distributed points against their X, Y positions from another (higher-accuracy) source. The error is generally specified as a circular error and estimated at the 95 percent confidence level according to the following formulation (Miller, 2013):

$$\text{Horizontal Accuracy} = 2.4477 * 0.5 * (\text{RMSEx} + \text{RMSEy}) \quad (2)$$

where RMSE is the root mean square error measured on the check points.

Table 11. Factors affecting acquisition efficiency and methods to shorten time.

Step	Issues	Methods and comments
Flight planning	Flight height above the ground (for a given GSD)	Fly as high as possible (this reduces the number of images, thus shortening both the acquisition and the post-processing time).
	Endlap	Classical AT (Aerial Triangulation) requires 57-65% overlap. If AT is skipped (replaced by direct georeferencing), this may be decreased, in order to limit the number of images (and shorten the post-processing time).
	Sidelap	Classical AT requires 30-40% overlap. If AT is skipped (replaced by direct georeferencing), this may be decreased, in order to limit the number of lines (and shorten the acquisition time).
	Flight speed	Plan it at the maximum permissible value (considering factors such as platform performances, forward motion compensation limits, standard speed according to economic and environmental issues, exposure time, image storage time, etc.)
	Geometry of AOI	If possible, select a rectangular AOI (this decreases the number of turns and increases the efficiency of the flight)
Flight	Turn pattern	"Short turn" is advisable against "smooth turn' (however, it depends on the pilot capacities and aircraft characteristics).
	IP (Initialization Point) time before image acquisition starts	Set it as small as possible (it depends on the pilot capacities and aircraft characteristics).

Table 12. Factors affecting postprocessing efficiency and methods to shorten time.

Step	Issues	Methods and comments
Tiff image generation	Number of bands (RGB, RGB+NIR, etc.)	Post-processing time increases with image size. The number of channels depend on the object that should be mapped. If possible, limit the number of channels and bits per band.
	Radiometric resolution (8, 16, 24 bits per pixel)	
Image orientation	Classical or GPS-assisted Aerial Triangulation (AT)	AT is time consuming, because it requires several operations to be performed (GCP – Ground Control Point field measurement, GCP measurement on images, bundle block adjustment). If accuracy requirements are not strict, AT can be skipped and replaced by DG. In this case, an additional calibration flight and misalignment computation should be included in the workflow; however the total time is shortened (see Section 4.2).
	Direct geo-referencing - DG (exterior orientation parameters derived from GNSS/IMU)	
Ortho-rectification	Overlay between images	Reduce it as much as possible
	Computation method	Choose a fast method, possibly with bilinear interpolation
Mosaicking	Seam line computation	The plain mosaic approach can be used: this avoids two operations, i.e. feature detection and seam applicator. Applying tiling avoid image generation in empty areas.
	Radiometry improvement	If possible, skip radiometry improvement procedures.

Table 13. Relevant case studies on post-disaster rapid mapping.

Reference	Type of disaster	Employed data	AOI	Method	Products	Delivery time
Hou et al., 2017	Mass movements	Pre-event: satellite images (QuickBird) and DEM Post-event: UAV images	Guanling County (China)	Photogrammetric processing (DEM and orthophoto generation), GIS spatial analysis tools and visual interpretation	(1D) terrain variation and (3D) morphological analysis managed on a web-GIS platform	-
Lei et al., 2017	Mass movements (earthquake-triggered)	UAV images	Sichuan province (China)	`Rapid image processing for geometric rectification and georeferencing.	Location and size of the landslides	-
Robinson et al., 2017	Mass movements (earthquake-triggered)	Satellite imagery (for samples mapping), DEM (for predisposing factors detection). No pre-event data is required.	Lesser Himalayan region (Nepal) 14,000 km^2	Fuzzy logic in GIS based on small samples of identified landslides	Location and relative magnitude of the landslides	Hours and days after the earthquake
Fernández et al., 2015	Mass movements	UAV images	La Guardia de Jaén (Spain) 250 x 100 m	Photogrammetric processing, comparison of observation campaigns	DSM, orthophoto	-
Dominici et al., 2017	Earthquake	UAV images	L'Aquila (Italy) – 3 case studies: square (60×40 m), single building, urban area	Photogrammetric and computer vision-based processing	3D point clouds and derived products (orthophoto, DSM, plans and sections).	-
Tamkuan et al., 2017	Earthquake	After-event satellite images (Landsat-8) and pre-, post-event satellite SAR data (ALOS-2)	Kumamoto (Japan)	Waterbodies and vegetation removal through optical images processing, damaged areas detection through normalized difference between pre- and post-event interferometric coherence. No training areas are required.	Classification maps with damaged buildings and landslides areas.	-
Ma et al., 2016	Earthquake	Pre- and post-event satellite images (GF-1 PMS-1 and PMS-2).	Center of Kathmandu (Nepal)	Fully automatic image processing based on Optimizable Variational model and SIFT constrained optical flow.	Cloudless backdrop maps, coarse change-detection maps and local temporal variation maps for key-areas.	46 min (cloudless map and coarse change map from 3 images)
Qi et al., 2016	Earthquake	UAV videos and images	Simulated case-studies and real earthquake in Lushan (China) 48.3 km2	Low-altitude statistical image processing methods based on motion/appearance analysis and similarity measurement.	On-line damaged building localization map.	39 hours for deployment, 11 hours of flight, 3 days of search&rescue.
Nex et al., 2014	Earthquake	Airborne images	San Felice sul Panaro (Italy) 2-3 ha	Photogrammetric processing + unsupervised classification approach	Classification maps (Fig. 4)	-
Li et al., 2017	Floods	25 pre-event satellite images (HJ-A/B), 48 post-event satellite images (HJ-A/B/C, SJ-9A); global open datasets in various formats (raster, vector and reports).	Myanmar 678,500 km^2	Flood extent estimation based on changes in pre- and post-flood water coverage; open-data integration as exposure elements to estimate the impacts of floods.	Maps of flood extent by state/province, affected towns, affected arable lands.	-
Rosser et al., 2017	Floods	Near-real-time satellite images (Landsat-8), geotagged crowdsourced images (Flickr), topographic data derived from available LiDAR DTM.	Oxford (UK) 154.35 km^2	Cumulative viewshed analysis (Flickr images), modified NDWI computation (Landsat-8 images), slope variable computation (DTM). Multi-source data fusion into a Bayesian statistical model.	Probabilistic flood map and flood extent map.	-
Alahacoon et al., 2016	Floods	SAR satellite data (ALOS PALSAR, RISAT, Radarsat-2, Sentinel-1, TERASAR, FORMOSAT), optical satellite images (Landsat-8 and FORMOSAT), UAV images	Kelani river basin (Sri Lanka) 2,500 km^2	SAR processing and image processing through the IWMI flood mapping tool.	Maps of flood extent at global scale (satellite data) and local scale (UAV data).	2-3 hours upon availability of satellite images from the Sentinel Asia network.

Table 13 *continued*. Relevant case studies on post-disaster rapid mapping.

Reference	Type of disaster	Employed data	AOI	Method	Products	Delivery time
Feng et al., 2015	Floods	UAV images	YuYao city (China) 10 km²	Photogrammetric processing.	Classification map	Few hours after the flight
Kakooei and Baleghi, 2017	Storms	Pre-disaster satellite images (from Google Earth); post-disaster satellite (from Google Earth), airborne (NOAA website) and UAV images (different sources).	Hurricane Irene, Hurricane Sandy, Illinois Tornado.	Automatic image processing for detection (and fusion) of buildings' roof damage from satellite images and buildings' façade damage from oblique airborne/UAV images.	Building damage estimation	-
Ferguson et al., 2016	Storms	UAV images and videos; ground-level panoramas	Southern New Brunswick (Canada)	Images uploading into a web-based interface to provide a fast assess of the site status; photogrammetric processing	Site overview through a web-based interface (for initial assessment); 3D model and orthophoto (for design phase and evaluation records)	Immediately after the data collection (web-interface); 1 week after data collection (3D model and ortho)
Hoque et al., 2016	Storms	Pre- and post-event satellite images (SPOT-5)	SARankhola Upazila (Bangladesh) 151.24 km2	Object-based classification technique to map land-cover types, followed by post-classification change detection.	Change detection maps and various change statistics (tables and graphs).	-
Jiang and Friedland, 2016	Storms	4-hrs post-event satellite images (IKONOS) and aerial images (NOAA)	Hurricane Katrina, Gulfport, Missisipi (USA) 900 x 630 m	Image classification, debris zone extraction and evaluation.	Debris zone maps and debris lines.	Depending on the classification approach, from 110 min to 160 min
Dunkel et al., 2017	Fire	Airborne SAR data and multi-sensor images (FLIR Star SAFIRE 380-HD camera system).	Southern California (USA) 36,000 acres	SAR and image processing.	Fire extent and direction of the fire line.	-
Kontoes et al., 2017	Fire	EO and non-EO satellite data (from NASA, NOAA and ESA missions), ASTER global DEM	Greek FireHub service – few examples over Greece are shown.	Several image processing solutions for hotspot detection (imagery classification and integration of a simulated fire dispersion model.	Thematic maps incl. damage assessments.	Fire extent provided every 5 min via the WebGIS interface
Hally et al., 2016	Fire	Satellite images (16-band Imager onboard Himawari-8)	North Cascade (Australia) 1800 ha	Robust matching algorithm, incl. least square error minimization and Kalman filtering.	Map of the fire spread.	-
Homainejad and Rizos, 2015	Fire	Integration of different UAV categories equipped with different sensors	-	Combination of different categories deployed in different airspaces	Multi-resolution data integration from EO, IR and SAR	-

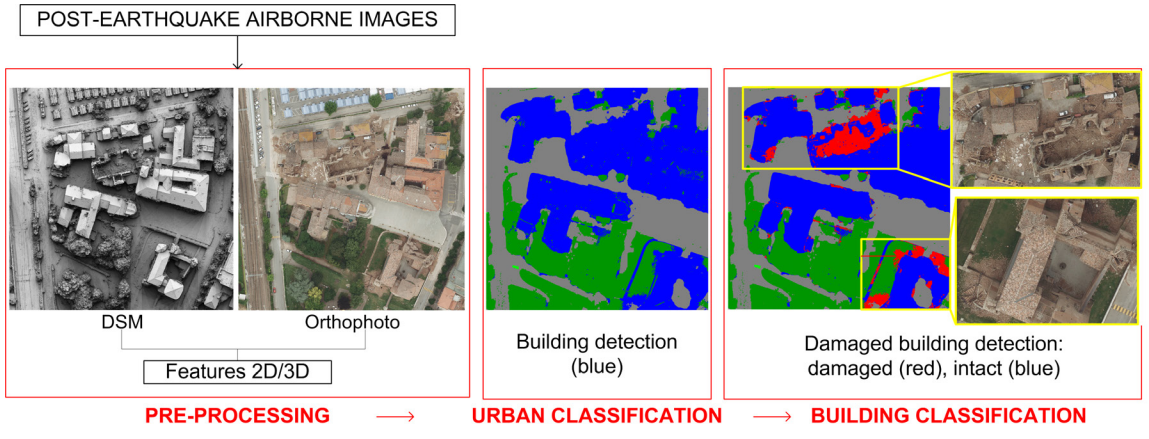

Figure 4. Workflow and results for mapping and classification of hazard areas (after Nex et al., 2014).

Literature Review

Relevant Case Studies on Post-Disaster Rapid Mapping

Table 13 summarizes a short review of rapid mapping activities based on satellite and airborne solutions. Because of the high volume of research work in this field, only few relevant case studies are collected for each type of disaster, focusing the attention on papers published in the last two to three years. Although incomplete and shortly outdated, this review includes relevant literature application examples that can support the choice of the most suitable technique. Among the others, an experience carried out by the authors is shown in Figure 4. It is part of the RapidMap project (http://rapidmap.fbk.eu), that built up a network of international researchers to address near real-time monitoring, change detection, mapping and data co-registration in case of hazards events (Baltsavias *et al.*, 2013).

Relevant Case Studies on Time Management

In order to provide valuable examples of airborne and UAV-based mapping applications and derive guidelines for an efficient time management, two relevant case studies are presented in the following.

Lucas (2015) evaluates issues affecting the production time for airborne orthophoto production and compares two alternative workflows, i.e., (a) the classical one, including aerial triangulation, ortho-rectification and advanced mosaicking methods, and (b) a shortened one, based on direct georeferencing. Table 14 summarizes the equipment and dataset used by the author, whereas Table 15 compares time values derived from the two processing approaches. The author also performs an accuracy assessment by measuring 15 control points on the final orthophotos. When the shortened process is adopted, RMSE values of 28 cm along X and 15 cm along Y are achieved. These values confirm typical literature results that usually point out a 1.5GSD accuracy level for the direct georeferencing approach (Mostafa, 2010). On the other hand, the AT-based workflow provides for a 1-GSD RMSE on the final orthophoto. Finally, a few guidelines are drawn:

- Most of the time is spared by replacing AT with DG (a 3:1 time ratio is expected). The calibration flight does not cost too much in terms of time, since it can be performed in parallel with other processes;
- An additional shortening can be gained by ending the workflow after the ortho-rectification;
- A suggested production strategy is to perform the traditional data acquisition procedure followed by two different post-processing approaches: a first one with the shortest workflow for faster disaster response (rush data) and a second one lasting longer and following a classical workflow with AT (optimal positional accuracy), enhanced radiometry and adequate work on seam lines;
- In the tests, each step of the process handles 100 percent of the imagery. A possible alternative may be the division of the dataset into subsets and the processing of the project in parts, with an efficient division of the AOI according to the needs of the disaster management authorities.

A typical UAV-based mapping scenario is discussed in (Boccardo *et al.*, 2015). In the framework of a UAV deployment exercise for rapid mapping purposes, the authors test three different workflows for an orthophoto production, based on (a) AT with GCPs measured by RTK GPS survey; (b) AT with GCPs measured by a GPS-equipped Smartphone and (c) DG, using data measured by the on-board GPS chip and attitude sensor. Table 16 summarizes the equipment and datasets used by the authors, whereas Table 17 compares time values derived from the different orthophoto production approaches. Finally, the accuracy of the ortho-rectified imagery is evaluated using the most accurate set of control points as reference values. Among the other results, it is worth stressing the significant performance achieved by the DG-based workflow: without any need of ground control, it provides for an average horizontal accuracy of about 1.5 m, which may perfectly fit the needs of the immediate response phase. Further useful remarks and guidelines drawn by the authors can be summarized as follows:

- Multi-rotor platforms represent the best mapping choice tests first choice for small and isolated areas or buildings, since they are more flexible if compared to fixed-wing platforms and can provide better GSD;
- When it comes to the survey of large areas, fixed-wing platforms speed up the acquisition time and should thus be preferred;

Table 14. Equipment and dataset used in the airborne mapping case study (Lucas, 2015).

Platform	Cesna 206 skywagon (Flight speed: 185 km/h)
Sensor	• RCD30 camera (Medium format digital camera - 60 MP. RGBN. Focal length: 53 mm. Pixel size: 6 µm, 9000*6732 pixels)
Hardware	• SGI Octane workstation (16 processors E5620 - Intel Xeon 2.4 GHz)
Software	• Framepro 1.3: tiff image generation • Leica IPAS_TC_3.2: trajectory computation; • Leica IPAS_CO_2.3: image orientation computation; • Trimble Inpho 6.0 Application Master: Block build-up; • Trimble Inpho 6.0 MATCH-AT: aerial triangulation; • Trimble Inpho 6.0 OrthoMaster: ortho-rectification; • Trimble Inpho OrthoVista: radiometric enhancement, mosaicking; • Trimble Inpho OrthoVistaSE: seam editing.
Dataset	• AOI: rectangular area of 447 km2; • Imagery: 1000 frames (15 cm GSD, 8 bits, 3 bands tiff images)

Table 15. Time values associated to the classical processing approach (AT including, second column) and shortened processing approach (AT skipped, third column). (*)DTM production time is not considered.

	Time values	
Step	*Workflow with AT*	*Workflow with DG*
Flight planning	20 min	20 min
Pilot mobilization	20 min	20 min
Data acquisition	2h 30min	2h 30min
Project download	1h 42min	1h 42min
Tiff image generation	3h 4min	3h 4min
Trajectory computation	20 min	20 min
Ext. orient. computation	5 min	5min
Creating block	5min	5min
GCP image measurement	1h 40min	-
GCP field measurement	4h	-
AT	8h	-
Ortho-rectification(*)	7h (150% overlay, cubic convolution, complete set of overview)	1h 44min (0% overlay, bilinear resampling, no overview)
Mosaicking	4h 38min (feature detection and seam applicator)	1h 17min (plain mosaic with tiling)
Calibration flight -CF	-	40min
Project download (CF)	-	10min
Tiff image generation (CF)	-	12min
Misalignment and camera calibration	-	30min
Total Time	33h 4min	10h 9min

- The more time-consuming steps are the initial ones, i.e., the initial briefing and the deployment of the team;
- To speed up the processing, besides the use of a DG-based workflow, it would be useful to minimize the number of images by means of automatic tools of image selection.

Conclusions

There are a number of different Geomatics solutions for approaching a rapid mapping task for any type of natural hazard event happened in a specific location. In many cases, the final decision on the data type and processing technique will depend on the equipment availability (platform and sensor), location and, sometimes, project funding. In order to assist the selection and decision-making processes, this research work provided a review of the current optical state-of-the-art remote sensing techniques (both satellite and airborne) for rapid mapping applications. Starting from the relevant information that should be gathered, several mapping options have been examined in order to collect and deliver a value-added and standardized output. The management of time has been defined as a priority and many solutions have been discussed in order to pursue efficiency in both data acquisition and processing. Finally, few relevant case studies have demonstrated the use of remote sensing techniques for post-disaster assessment and proposed strategies for fast data acquisition and processing.

Table 16. Equipment and dataset used in the UAV-based mapping case study (Boccardo *et al.*, 2015).

Platform and sensor	• Hexakopter by MikroKopter equipped with Sony Nex 5 (16mm focal length). • eBee by SenseFly fixed-wing platform equipped with Canon Ixus (4.3mm focal length).
Hardware	-
Software	PhotoScan by Agisoft
Dataset	AOI: rectangular area of 1.5 km^2; • Imagery (Hexakopter): 190 frames (0.022 m GSD) at flight height of 70m; 120 frames (0.05 m GSD) at flight height of 150m; • Imagery (eBee): 160 frames (0.05 m GSD) at flight height of 150m.

Bearing these lessons in mind, few final remarks can be drawn:

- Thanks to their increased spatial, spectral and temporal resolution, satellite observations can today provide for a regular, consistent (i.e., systematically collected and standardized), and detailed update on the status of hazards at multiple scales, from global to local levels. Furthermore, the development and maintenance of international programs for data open-access and sharing, makes the availability of satellite data always more immediate also for inaccessible, remote and hazardous areas;
- The airborne remote sensing industry is recently experiencing an unprecedented diversity in the development of platforms and sensors. Many types of platform exist, both manned and unmanned, that enable sensors (usually, high-performance medium-format digital cameras) to access remote and denied areas at close-to-target altitudes;
- Within the airborne scenario, the use of helicopters (sometimes associated with hand-held acquisition systems) and UAVs usually represents the most flexible means of data acquisition. In particular, UAVs can deal with the problem of site accessibility and operator security, and show the best performance in terms of spatial resolution and viewing directions;
- Thus, data and technologies are mainly available and the major challenges today concern the efficient selection (and integration) of the most fit-for-purpose mapping solution(s) and the development of automatic procedures to increase efficiency in data processing;
- On one hand, real-time information transfer, real-time imagery geo-referencing and the adaptation of the sensors to the payload allowed by UAV platforms are expected to made this technology an efficient mapping means for post-disaster assessment. On the other hand, a number of open issues should be solved, such as those concerning platform stability, limitations in terms of area coverage, endurance, and direct georeferencing;
- In particular, the latter represents the most promising strategy to increase efficiency in data processing. However, the accuracy of results delivered by the DG approach is still questionable; it mainly derives from the performance of embedded navigation system, those of the platform adopted and from the solution used for sensor synchronization.

Table 17. Time values associated to different processing approaches. Deployment time is not included in the total time computation. (*) Measured by a GPS-equipped smartphone; (**) DTM production time is not considered.

	Time values					
Step	*Hexakopter flight H.70m phone(*) GCPs*	*Hexakopter flight H.70m RTK GCPs*	*Hexakopter, flight H.150m phone(*) GCPs*	*Hexakopter, flight H.150m RTK GCPs*	*eBee, flight H.150m* DG	*eBee, flight H.150m RTK GCPs*
Initial briefing	30-45min	30-45min	30-45min	30-45min	30-45min	30-45min
Deployment of the team in the affected area	few hrs	few hrs	few hrs	few hrs	few hrs	few hrs
UAV system setup	20min	20min	20min	20min	20min	20min
GCP positioning and survey	45min	55min	45min	55min	-	55min
Flight planning	10min	10min	5min	5min	10min	10min
Flight	13min	13min	9min	9min	17min	17min
Data download	5min	5min	5min	5min	5min	5min
Data processing(**) (orthophoto production)	1h 30min	1h 30min	1h 25min	1h 25min	1h 40min	1h 50min
Data dissemination (web map server)	10min	10min	10min	10min	10min	10min
Total Time	3h 53min	4h 3min	3h 39min	3h 49min	3h 22min	4h 27min

References

Abdullah, Q.A., 2013. Photogrammetric platforms, *Manual of Photogrammetry* (J. Chris McGlone, editor), ASPRS, Sixth Edition, pp. 1318.

Alahacoon, N., P. Pani, K. Matheswaran, S. Samansiri, G Amarnath, S. Balasubramanya, M.C. Buisson, P. Saikia, K. MacDonald, S. Aslamy, and T. Horbulyk, 2016. Rapid emergency response mapping for the 2016 floods in Kelani river basin, Sri Lanka, *Proceedings of the 37th ACRS Conference*, Colombo, Sri Lanka.

Baltsavias, E., K. Cho, F. Remondino, U. Soergel, and H. Wakabayashi, 2013. Rapidmap - Rapid mapping and information dissemination for disasters using remote sensing and geoinformation, *ISPRS Archives of the Photogrammetry, Remote Sensing and Spatial Information Sciences*, 40(7/W2):31–35.

Boccardo, P., 2016. Geomatics and Emergency Management Workshop "Multidisciplinary and transnational applications of Geomatics", *Proceedings of the SIFET Annual Conference*.

Boccardo, P., F. Chiabrando, F. Dutto, F.G. Tonolo, and A. Lingua, A., 2015. UAV deployment exercise for mapping purposes: Evaluation of emergency response applications, Sensors, 15(7):15717–15737.

Calvari, S., L. Lodato, and L. Spampinato, 2004. Monitoring active volcanoes using a handheld thermal camera, *Proceedings of Thermosense XXVI-SPIE*, The International Society for Optical Engineering.

Casagli, N., W. Frodella, S. Morelli, V. Tofani, A. Ciampalini, E. Intrieri, F. Raspini, G. Rossi, L. Tanteri, and P. Lu, 2017. Spaceborne, UAV and ground-based remote sensing techniques for landslide mapping, monitoring and early warning, *Geoenvironmental Disasters*, 4(1):9.

CEOS Database, URL: http://database.eohandbook.com/ (last date accessed: 09 November 2017).

CEOS, 2015. Satellite earth observations in support of disaster risk reduction, URL: http://www.eohandbook.com (last date accessed: 09 November 2017)).

Chiabrando, F., G. Sammartano, and A. Spanò, 2017. A comparison among different optimization levels in 3D multi-sensor models, A test case in emergency context: 2016 Italian earthquake, *ISPRS-International Archives of the Photogrammetry, Remote Sensing and Spatial Information Sciences*, pp.155–162.

Colomina, I., and P. Molina, 2014. Unmanned aerial systems for photogrammetry and remote sensing: A review, *ISPRS Journal of Photogrammetry and Remote Sensing*, 92:79–97.

Coltelli, M., P.J. d'Aranno, R. de Bonis, J.F. Guerrero-Tello, M. Marsella, C. Nardinocchi, E. Pecora, C. Proietti, S. Scifoni, M. Scutti, and W. Wahbeh, 2017. The Use of surveillance cameras for the rapid mapping of lava flows: An application to Mount Etna Volcano, *Remote Sensing*, 9(3):192.

Copernicus EMS, Emergency Management Service, URL: emergency.copernicus.eu/mapping, (last date accessed: 09 November 2017).

Dominici, D., M. Alicandro, and V. Massimi, 2017. UAV photogrammetry in the post-earthquake scenario: case studies in L'Aquila, *Geomatics, Natural Hazards and Risk*, 8(1):87–103.

Dunkel, R., R. Saddler, and A.W. Doerry, 2017, Use of unmanned SAR and EO/IR sensor suites for monitoring wildfires, *SPIE Defense+ Security*, International Society for Optics and Photonics, pp. 101881F–101881F

Edwards, E., E. Frey, P.A. Jones, R.K. Jungquist, A.G. Lareau, J. Lebarron, C.S. King, K. Komazaki, C. Toth, S. Walker, E.F. Whittaker, P. Zavattero, and H. Zuegge, 2013. Cameras and sensing systems, *Manual of Photogrammetry* (J. Chris McGlone, editor), ASPRS, Sixth edition, pp. 1318.

EFAS. European Flood Awareness System, URL: www.efas.eu (last date accessed: 09 November 2017).

EFFIS. European Forest Fire Information System, URL: forest.jrc.ec.europa.eu/effis (last date accessed: 09 November 2017).

Emergency Mapping Guidelines, 2015. International Working Group on Satellite-based Emergency Mapping (IWG-SEM), URL: http://www.un-spider.org/network/iwg-sem (last date accessed: 09 November 2017).

eoPortal - https://directory.eoportal.org/web/eoportal/satellite-missions (last date accessed: 09 November 2017).

Erdelj, M., M. Król, and E. Natalizio, 2017. Wireless sensor networks and multi-UAV systems for natural disaster management, *Computer Networks*.

F. Nex, E. Rupnik, I. Toschi, and F. Remondino, 2014: Automated processing of high resolution airborne images for earthquake damage assessment, *ISPRS Archives of the Photogrammetry, Remote Sensing and Spatial Information Sciences*, Vol. XL-1, pp. 315–321.

Feng, Q., J. Liu, and J. Gong, 2015. Urban flood mapping based on unmanned aerial vehicle remote sensing and random forest classifier - A case of Yuyao, China, *Water*, 7(4):1437– 1455.

Ferguson, L.D., L. Miller, M. Wolfe, J. McGinn, and L. Waugh, 2016. NDM-523: Use of an unmanned aerial vehicle (UAV) to assess transportation infrastructure immediately after a catastrophic storm event.

Fernández, T., J.L. Pérez, F.J. Cardenal, A. López, J.M. Gómez, C. Colomo, J. Delgado, and M. Sánchez, 2015. Use of a light UAV and photogrammetric techniques to study the evolution of a landslide in Jaén (southern Spain), *The International Archives of Photogrammetry, Remote Sensing and Spatial Information Sciences*, 40(3):241.

Flood, M., 2001. Laser altimetry: From science to commercial LIDAR mapping, *Photogrammetric Engineering & Remote Sensing*, 67(11).

Gillespie, T.W., J. Chu, E. Frankenberg, and D. Thomas, 2007. Assessment and prediction of natural hazards from satellite imagery, *Progress in Physical Geography*, 31(5):459–470.

GIM-International UAS edition, 2016, URL: www.geo-matching.com/category/id64-uas-for-mapping-and-3D-modelling.html (last date accessed 09 November 2017).

Gomez, C., and H. Purdie, UAV-based photogrammetry and geocomputing for hazards and disaster risk monitoring–A review, *Geoenvironmental Disasters*, 3(1):23. 2016.

Grenzdörffer, G., 2008. Medium format digital cameras, A EuroSDR project, *The International Archives of Photogrammetry, Remote Sensing and Spatial Information Sciences*, Vol. 37, pp.1043–1050.

Hally, B., L. Wallace, K. Reinke, and S. Jones, 2016. Assessment of the utility of the advanced Himawari Imager to detect active fire over Australia, *The International Archives of the Photogrammetry, Remote Sensing & Spatial Information Sciences*, 41.

Homainejad, N. and C. Rizos, 2015. Application of multiple categories of Unmanned Aircraft Systems (UAS) in different airspaces for bushfire monitoring and response, *The International Archives of Photogrammetry, Remote Sensing and Spatial Information Sciences*, 40(1):55

Hoque, M.A.A., S. Phinn, C. Roelfsema, and I. Childs, 2016. Assessing tropical cyclone impacts using object-based moderate spatial resolution image analysis: A case study in Bangladesh, *International Journal of Remote Sensing*, 37(22):5320–5343.

Hoque, M.A.A., S. Phinn, C. Roelfsema, and I. Childs, I., 2017. Tropical cyclone disaster management using remote sensing and spatial analysis: a review, *International Journal of Disaster Risk Reduction*.

Hou, W., X. Lu, P. Wu, A. Xue, and L. Li, 2017. An integrated approach for monitoring and information management of the Guanling landslide (China), *ISPRS International Journal of Geo-Information*, 6(3):79.

Jiang, S., and C.J. Friedland, 2016. Automatic urban debris zone extraction from post-hurricane very high-resolution satellite and aerial imagery, *Geomatics, Natural Hazards and Risk*, 7(3):933-952.

Joyce, K.E., S.E. Belliss, S.V. Samsonov, S.J. McNeill, and P.J. Glassey, 2009b. A review of the status of satellite remote sensing and image processing techniques for mapping natural hazards and disasters, *Progress in Physical Geography*, 33(2):183–207.

Joyce, K.E., S.V. Samsonov, S.R. Levick, J. Engelbrecht, and S. Belliss, 2014. Mapping and monitoring geological hazards using optical, LiDAR and synthetic aperture RADAR image data, *Natural Hazards*, 73(2):137–163.

Joyce, K.E., K.C. Wright, S.V. Samonsov, V.G. Ambrosia, 2009a. Remote sensing and the disaster management cycle, *Advances in Geoscience and Remote Sensing* (G. Jedlovec, editor), In-Tech Publishing, Vienna, pp. 317–346.

Kakooei, M., and Y. Baleghi, 2017. Fusion of satellite, aircraft, and UAV data for automatic disaster damage assessment, *International Journal of Remote Sensing*, 38(8-10):2511–2534.

Klonner, C., S. Marx, T. Usón, J. Porto de Albuquerque, and B. Höfle, 2016. Volunteered geographic information in natural hazard analysis: A systematic literature review of current approaches with a focus on preparedness and mitigation, *ISPRS International Journal of Geo-Information*, 5(7):103.

Kontoes, C., I. Papoutsis, T. Herekakis, E. Ieronymidi, and I. Keramitsoglou, 2017. Remote sensing techniques for forest fire disaster management: The FireHub operational platform, *Integrating Scale in Remote Sensing and GIS*, p.157.

Larson, W.J., and J.R. Wrttz, 1999. *Space Mission Analysis and Design*, Third edition, Kluver Academic Publisher, pp. 969.

Lei, T., Y. Zhang, X. Wang, L. Li, Z. Pang, X. Zhang, and G. Kan, 2017, The application of unmanned aerial vehicle remote sensing for monitoring secondary geological disasters after earthquakes, *Proceedings of the Ninth International Conference on Digital Image Processing (ICDIP 2017)*, International Society for Optics and Photonics, pp. 104203H–104203H

Li, S., Y. Cui, M. Liu, H. He, and S. Ravan, 2017. Integrating global open geo-information for major disaster assessment: A case study of the Myanmar Flood, *ISPRS International Journal of Geo-Information*, 6(7):201.

Lucas, G., 2015. Considering time in orthophotography production: From a general workflow to a shortened workflow for a faster disaster response, *The International Archives of Photogrammetry, Remote Sensing and Spatial Information Sciences*, Vol. XL-3/W3:249–255.

Ma, Y., F. Chen, J. Liu, Y. He, J. Duan, and X. Li, 2016. An automatic procedure for early disaster change mapping based on optical remote sensing, *Remote Sensing*, 8(4):272.

Malehmir, A., L.V. Socco, M. Bastani, C.M. Krawczyk, A.A. Pfaffhuber, R.D. Miller, H. Maurer, R. Frauenfelder, K Suto, S. Bazin, and K. Merz, 2016. Chapter two-near-surface geophysical characterization of areas prone to natural hazards: A review of the current and perspective on the future, *Advances in Geophysics*, 57:51–146.

Miller, S., 2013. Photogrammetric products, *Manual of Photogrammetry* (J. Chris McGlone editor), ASPRS, Sixth edition, pp. 1318

Molinari, D., S. Menoni, and F. Ballio (editors)., 2017. *Flood Damage Survey and Assessment: New Insights from Research and Practice*, John Wiley & Sons.

Mostafa, M.M.R., and J. Hutton, 2010. Theoretical ground accuracy analysis derived from today's airborne digital frame cameras and direct georeferencing, *Proceedings of the ASPRS 2010 Annual Conference*, San Diego, California, April 26-30 2010.

Nedjati, A., B. Vizvari, and G. Izbirak, 2016. Post-earthquake response by small UAV helicopters, *Natural Hazards*, 80(3):1669–1688.

Nex, F., and F. Remondino, 2014. UAV for 3D mapping applications: A review, *Applied Geomatics*, 6(1):1–15.

Nex, F., E. Rupnik, I. Toschi, and F. Remondino, 2014. Automated processing of high resolution airborne images for earthquake damage assessment, *The International Archives of Photogrammetry, Remote Sensing and Spatial Information Sciences*, 40(1):315.

Perez-Mato, J., V. Arana, and F. Cabrera-Almeida, 2016. Real-time autonomous wildfire monitoring and georeferencing using rapidly deployable mobile units, *IEEE Aerospace and Electronic Systems Magazine*, 31(2):6–15.

Petrides, P., P. Kolios, C. Kyrkou, T. Theocharides, and C. Panayiotou, 2017. Disaster prevention and emergency response using unmanned aerial systems, *Smart Cities in the Mediterranean*, Springer International Publishing, pp. 379–403

Petrie, G., 2010. Current developments in airborne digital frame cameras: As displayed in the Intergeo 2010 exhibition, *GeoInformatics*, 13(8):34–40.

Qi, J., D. Song, H. Shang, N. Wang, C. Hua, C. Wu, X. Qi, and J. Han, 2016. Search and rescue rotary-wing UAV and its application to the Lushan Ms 7.0 earthquake, *Journal of Field Robotics*, 33(3):290–321.

Remondino, F., and M. Gerke, 2015. Oblique aerial imagery - A Review, *Proceedings of Photogrammetric Week 2015* (Dieter Fritsch, editor), pp. 75–83.

Remondino, F., 2011. Heritage recording and 3D modeling with photogrammetry and 3D scanning, *Remote Sensing*, 3(6):1104–1138.

Remondino, F., I. Toschi, M. Gerke, F. Nex, D. Holland, A. McGill, J. Talaya Lopez, and A. Magarinos, 2016. Oblique aerial imagery from NMA - Some best practices, *The International Archives of Photogrammetry, Remote Sensing and Spatial Information Sciences* Vol. XLI, in press.

Robinson, T.R., N.J. Rosser, A.L. Densmore, J.G. Williams, M.E. Kincey, J. Benjamin, and H.J. Bell, 2017. Rapid post-earthquake modelling of coseismic landslide magnitude and distribution for emergency response decision support, *Natural Hazards and Earth System Sciences Discussions*, pp.1–29.

Rosser, J.F., D.G. Leibovici, and M.J. Jackson, 2017. Rapid flood inundation mapping using social media, remote sensing and topographic data, *Natural Hazards*, 87(1):103-120.

Skaloud, J., J. Vallet, K. Keiler, G. Veyssière, and O. Kolbl, 2006. Rapid aerial mapping with handheld sensors, *GPS World*.

Smith, M.W., J.L. Carrivick, J. Hooke, and M.J. Kirkby, 2014. Reconstructing flash flood magnitudes using 'Structure-from-Motion': A rapid assessment tool, *Journal of Hydrology*, 519:1914–1927.

Tamkuan, N., and M. Nagai, 2017. Fusion of multi-temporal interferometric coherence and optical image data for the 2016 Kumamoto earthquake damage assessment, *ISPRS International Journal of Geo-Information*, 6(7):188.

The International Disaster Charter, URL: www.disasterscharter.org (last date accessed 09 November 2017)

Tralli, D.M., R.G. Blom, V., A. Donnellan, and D.L. Evans, 2005. Satellite remote sensing of earthquake, volcano, flood, landslide and coastal inundation hazards, *ISPRS Journal of Photogrammetry and Remote Sensing*, 59(4):185–198.

UNEP - United Nations Environment Programme, 2012. Early warning systems: A state of the art analysis and future directions, Division of Early Warning and Assessment (DEWA), United Nations Environment Programme (UNEP).

UN-SPIDER- United Nations Platform "Space-based Information for Disaster management and Emergency Response", URL: http://www.un-spider.org/space-application-matrix (last date accessed: 09 November 2017).

Vallet, J. and J. Skaloud, 2004. Development and experiences with a fully-digital handheld mapping system operated from a helicopter, *International Archives of the Photogrammetry, Remote Sensing and Spatial Information Sciences*, 35:1–6.

Voigt, S., F. Giulio-Tonolo, J. Lyons, J. Ku-era, B. Jones, T. Schneiderhan, G. Platzeck, K. Kaku, M.K. Hazarika, L. Czaran, and S. Li, 2016. Global trends in satellite-based emergency mapping, *Science*, 353(6296):247–252.